Janus Nanostructures Based on Au–TiO$_2$ Heterodimers and Their Photocatalytic Activity in the Oxidation of Methanol

Sulolit Pradhan,[†] Debraj Ghosh,[‡] and Shaowei Chen*

Department of Chemistry and Biochemistry, University of California, 1156 High Street, Santa Cruz, California 95064

ABSTRACT Au–TiO$_2$ snowman-like heterodimer nanoparticles were prepared by a surface sol–gel process based on gold Janus nanoparticles whose surface-protecting monolayers consisted of a hemisphere of hydrophobic 1-hexanethiolates and the other of hydrophilic 2-(2-mercaptoethoxy)ethanol. Transmission electron microscopic measurements showed that the resulting TiO$_2$ nanoparticles (diameter 6 nm) exhibited well-defined lattice fringes that were consistent with the (101) diffraction planes of anatase TiO$_2$. The heterodimer nanoparticles displayed apparent photoluminescence that was ascribed to electronic transitions involving trap states of TiO$_2$ particles, and the photocatalytic activity was manifested by the oxidative conversion of methanol into formaldehyde, which was detected quantitatively by the Nash method. The enhanced photocatalytic performance, as compared to that of the TiO$_2$ nanoparticles alone, was ascribed to the charge separation of photogenerated electrons and holes at the Au–TiO$_2$ interface that was facilitated by the close proximity of the gold nanoparticles. These results suggested that (i) there were at least two possible pathways for photogenerated electrons at the TiO$_2$ conduction band, decay to the trap states and transfer to the gold nanoparticles, and (ii) energy/electron transfer from the trap states to gold nanoparticles was less efficient. In essence, this study showed that the snowman-like heterodimers might be exploited as a homogeneous photocatalytic system for the preparation of functional molecules and materials.

KEYWORDS: Janus nanoparticle • Au-TiO$_2$ heterodimer • surface sol–gel • photocatalysis • methanol oxidation • Nash method

INTRODUCTION

Nanosized metal oxide particles have been used extensively as active components in photocatalysis, photovoltaics, and electrochromic devices, as well as chemical and biological sensors, largely because of their large band-gap energy, corrosion resistance, mechanical durability, and abundant availability (and, hence, low costs) (1–6). Of these, titanium dioxide (TiO$_2$) has attracted particular attention. TiO$_2$ exhibits a band-gap energy of ca. 3 eV and has been known to exist in at least three different crystalline phases, anatase, rutile, and brookite, of which the anatase phase has been found to be the most active in photocatalysis (7–9). The photocatalytic activity of TiO$_2$ was first illustrated by Fujishima and Honda in 1972 when they demonstrated that water hydrolysis might be initiated by TiO$_2$ under photoirradiation (10). This was accounted for by the formation of electron–hole pairs upon photoexcitation by photons with energy larger than the material band gap, where the separation of the charges was exploited for the reduction and oxidation of water. This fundamental principle of photogenerated electrons and holes has now been extended to a wide array of applications, such as solar energy conversion (photovoltaics), degradation of organic pollutants, transformative production of organic functional compounds, fuel cell electrochemistry, and antibacterial protection (11–14).

However, the photocatalytic efficiency by TiO$_2$ alone is generally rather poor. One effective strategy to enhance the catalytic performance is to couple the oxide materials with metal nanoparticles. This is primarily motivated by the enhanced efficiency of interfacial charge separation because metal nanoparticles are, in general, good electron sinks as a consequence of the significantly larger Helmhotz double-layer capacitance than the space charge capacity of the oxide particles even under accumulation. This accumulation of photogenerated electrons helps impede the recombination dynamics (15).

Toward this end, a variety of synthetic routes have been reported in the literature. For instance, a composite with gold nanorods trapped within a TiO$_2$ hollow shell has been prepared and found to serve as effective catalysts in the reduction of Fe(CN)$_6^{3-}$ by NaBH$_4$ (16). Yang and co-workers used a surface sol–gel method to prepare ultrathin TiO$_2$ films that served as the supporting matrix for gold nanoparticles (17). The resulting nanocomposites were found to be active in low-temperature CO oxidation. In another study (18), an amorphous TiO$_2$ shell was grown onto gold nanoparticle surfaces by a sol–gel method, leading to the formation of core–shell Au@TiO$_2$ nanocomposites. Core–shell Au@TiO$_2$ nanocomposites were also prepared by a hydrothermal technique (19), where the (101) planes of TiO$_2$ were found to grow preferentially on the surface of gold nanopar-

Scheme 1. Schematic of the Formation of Au−TiO₂ Heterodimer Nanoparticles
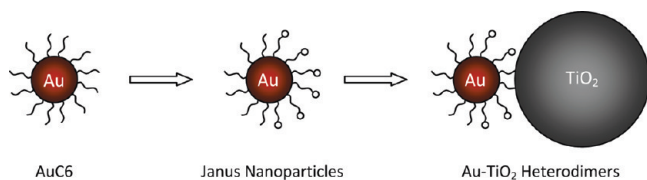
ticles and stabilize the heterointerfaces. The photocatalytic activity was demonstrated by the oxidation of acetaldehyde. Armelao et al. (20) deposited nanosized gold particles onto a TiO₂ sol−gel surface by radio-frequency sputtering and evaluated the photocatalytic activity with the photodecomposition of an azo dye (plasmocorinth B). The deposition of metal nanoparticles (silver and gold) onto TiO₂ particle surfaces has also been achieved by the photoreduction of metal salt precursors (21). In some other studies, the metal−TiO₂ nanocomposites have been prepared by the direct incorporation of metal nanoparticles into the oxide matrixes. For instance, gold nanoparticles may be dispersed into a titanium sol−gel precursor, where gelation leads to the embedment of the gold nanoparticles into a titania dielectric matrix (22, 23). In another study, Au−TiO₂ nanocomposites were formed by sol−gel reactions of titanium tetraisopropoxide with HAuCl₄ in a triblock copolymer template, where calcination at elevated temperatures led to the formation of gold nanoparticles embedded in the TiO₂ network (24). The photocatalytic activity was manifested in methanol oxidation. Additionally, a nanocomposite based on silver nanoparticles stabilized by anatase TiO₂ nanorods has been used in the photocatalysis of reductive bleaching of a model dye (Uniblue A) (15).

It should be noted that, in these earlier studies, TiO₂ is typically prepared by the sol−gel route and, hence, the size is generally at least a few tens of nanometers (up to a few micrometers); additionally, the resulting metal−TiO₂ nanocomposites are mostly involved in heterogeneous catalytic reactions largely because the materials are not dispersible in common solvent media. This severely limits the contact area and, hence, the catalytic performance.

Thus, in this study, we present a novel approach based on gold Janus nanoparticles for the preparation of Au−TiO₂ nanocomposite particles. Specifically, amphiphilic gold nanoparticles will first be prepared by interfacial ligand-exchange reactions, where the hydroxyl functional groups on the hydrophilic hemisphere are exploited as anchoring sites for the growth of TiO₂ nanoparticles, leading to the formation of a snowman-like heterodimer nanoparticle (Scheme 1). The unique advantages of this preparative route, as compared to the previous ones, mainly lie in two aspects: the exact pairing alignment between the metal and TiO₂ nanoparticles for efficient charge separation and accumulation and the ready dispersion of the heterodimers in common solvent media, which provides a chemical environment equivalent to that of homogeneous reactions as well as ready spectrophotometric detections and

monitoring of the reaction processes. We will use methanol photooxidation into formaldehyde as the illustrating example, by using the Nash method (25) to examine the reaction dynamics. Note that selective oxidation is important in the synthesis of fine chemicals and intermediates. Of these, the oxidation of primary alcohols to aldehydes is a fundamentally important procedure in laboratory and commercial research (26−28). The photocatalytic performance of commercial TiO₂ particles is also evaluated and compared.

EXPERIMENTAL SECTION

Chemicals. Hydrogen tetrachloroauric acid (HAuCl₄ · xH₂O) was synthesized by dissolving ultrahigh-purity gold (99.999 %, Johnson Matthey) in freshly prepared aqua regia followed by crystallization (29). Tetraoctylammonium bromide (Alfa Aesar, 98 %), 1-hexanethiol (C6SH; Acros, 96 %), sodium borohydride (NaBH₄; Acros, 99 %), titanium butoxide (Acros, 98+ %), acetylacetone (acac; Pfaltz and Bauer, 98 %), ammonium acetate (NH₄Ac; Fisher Chemicals), and titanium dioxide nanoparticles (TiO₂; average diameter 25 nm, Aldrich) were all used as received. 2-(2-Mercaptoethoxy)ethanol (MEA; HSCH₂CH₂OCH₂CH₂OH) was synthesized and characterized according to a literature procedure (30). Other solvents were purchased from typical commercial sources at their highest purity and used without further treatment. Water was supplied by a Barnstead Nanopure water system (18.3 MΩ cm).

Gold Janus Nanoparticles. Gold Janus nanoparticles, with one hemisphere passivated by hydrophobic hexanethiolates and the other by hydrophilic MEA ligands, were prepared by following a procedure detailed previously (31). Briefly, 1-hexanethiolate-protected gold (AuC6) particles were first synthesized and purified by using the Brust protocol (32). The particles then underwent fractionation by using a mixture of toluene and ethanol (33, 34), and the fraction with an average core diameter of 2.0 nm (corresponding approximately to a particle composition (35) of Au₃₁₄C6₉₁) was used for the subsequent study.

A monolayer of the AuC6 nanoparticles was then formed on the water surface of a Langmuir−Blodgett trough (NIMA Technology, model 611D). At a high surface pressure, the particle monolayer was deposited by the Langmuir−Blodgett technique onto a clean microscope glass slide, which was then immersed into a water solution of 1 mM MEA that was kept in a water circulation bath with the temperature set at 45 °C. The exchange reactions were found to occur only at the top face of the particles, which was in direct contact with the water phase, thereby producing Janus nanoparticles. At least four batches of particle samples were prepared and collected under identical conditions to provide a large sample size for further functionalization. The resulting Janus particles were found to be soluble in dichloromethane, chloroform, and tetrahydrofuran (THF). ¹H NMR measurements showed that the particle protecting layer consisted of approximately 45 % MEA and 55 % hexanethiolate ligands (31).

Au−TiO₂ Heterodimer Nanostructures. The hydroxyl functional groups on the gold Janus nanoparticle surface were then exploited as the anchoring sites for the growth of TiO₂ nanoparticles by a surface sol−gel process, leading to the formation of Au−TiO₂ snowman-like heterodimer nanostructures (Scheme 1). In a typical experiment, 1.5 mg of the gold Janus particle was dissolved in a mixture of deaerated THF and methanol [1:1 (v/v); total volume 2 mL], which was designated as solution A. Separately, 1.0 mL of titanium butoxide was mixed with 1.6 mL of acac. To this solution was added 1.2 mL of deaerated methanol, and the reaction was allowed to run for 30 min under

a nitrogen atmosphere. This solution was designated as solution B. Solutions A and B were then mixed and subjected to vigorous magnetic stirring for 2 h under a nitrogen atmosphere. After this, the solution was dried and washed extensively with deaerated methanol to remove any excessive alkoxide precursors. The particles were then dispersed into degassed water for 20 min, dried with nitrogen, and rinsed with deaerated methanol, affording purified Au—TiO$_2$ heterodimer nanoparticles. Approximately 1.2 mg of the product was obtained and found to have good solubility in various organic solvents such as CH$_2$Cl$_2$, CHCl$_3$, and THF.

Transmission Electron Microscopy (TEM). The nanoparticle structures were examined with a Philips CM200/FEG high-resolution transmission electron microscope operated at 200 kV at the Molecular Foundry, National Center for Electron Microscopy, at Lawrence Berkeley National Laboratory. The samples were prepared by casting a drop of the particle solution (∼1 mg/mL) in dichloromethane onto a 200-mesh carbon-coated copper grid. The particle core diameter was estimated by using *ImageJ* software analysis of the TEM micrographs.

Spectroscopy. UV—vis spectra were acquired with a UNICAM ATI UV4 spectrometer at a particle concentration of 0.1 mg/mL in the reaction solution using a 1 cm quartz cuvette. Photoluminescence measurements were carried out with a PTI fluorescence spectrometer using the same solutions as those for UV—vis measurements.

Photocatalytic Oxidation of Methanol. In a typical experiment, 1.0 mg of the Au—TiO$_2$ heterodimer nanoparticles was dissolved in a mixture of THF and water (1:1 by volume; total volume 20 mL). To this were added 0.01 M acac, 0.33 M NH$_4$Ac, and 0.62 mM of methanol, and the solution was mixed by vigorous magnetic stirring. The resulting solution was saturated with oxygen by bubbling ultrapure oxygen into the solution for 5 min. Then, the solution was subject to photoirradiation with UV light (365 nm, 6 W) under a nitrogen atmosphere. An aliquot of 2.5 mL was taken out of the solution at varied time intervals for UV—vis measurements. The reaction was allowed to run until steady state was observed in the spectral profile. A control experiment was also carried out with commercially available TiO$_2$ nanoparticles under otherwise identical experimental conditions.

RESULTS AND DISCUSSION

The structures of the Au—TiO$_2$ heterodimers were first characterized by TEM measurements. Figure 1 depicts two representative TEM micrographs at different resolutions. In panel A, a relatively long-range-ordered array of nanoparticles can be seen, which essentially consists of two kinds of particles. The ones with a darker contrast exhibit a diameter of ca. 2 nm and are ascribed to gold nanoparticles, whereas the lighter-contrast ones, with a diameter of about 6 nm, are attributable to the TiO$_2$ nanoparticles. The pairing of the gold and TiO$_2$ nanoparticles is better resolved in panel B, as highlighted in white circles, where the interparticle distance (<0.6 nm) is smaller than the fully extended chain length of the MEA ligands (0.75 nm as evaluated by Hyperchem). Furthermore, the lattice fringes of 0.36 nm are very well-defined in the larger particles (red lines), which are consistent with the (101) diffraction planes of anatase TiO$_2$. It should be noted that, although the TiO$_2$ nanoparticles were prepared at room temperature and without any postsynthesis (calcination) treatment, the particles exhibit a remarkable level of purity in the crystalline phase. This is in sharp contrast to a number of earlier studies where the TiO$_2$
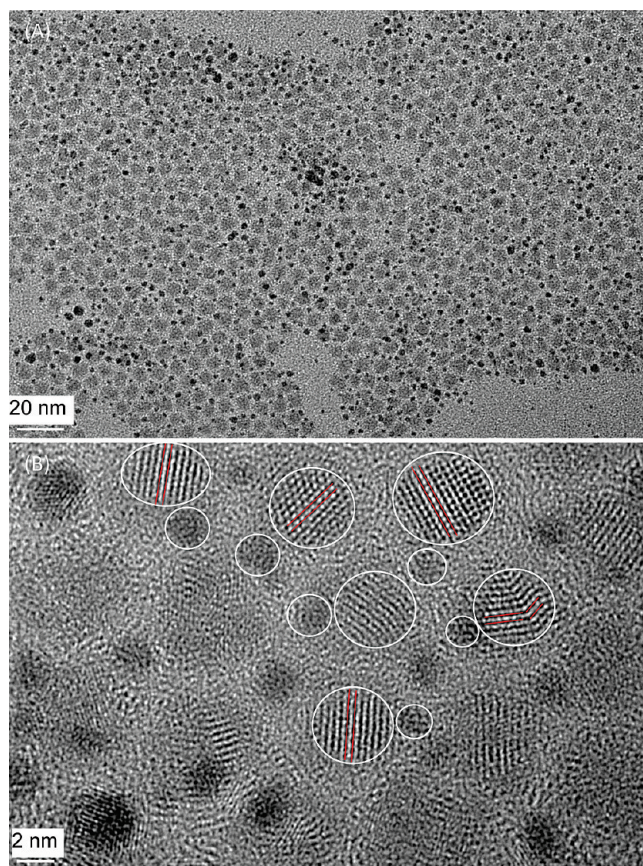
FIGURE 1. TEM micrographs of Au—TiO$_2$ heterodimer nanoparticles. The scale bar is 20 nm in panel A and 2 nm in panel B. The lattice fringes of TiO$_2$ are highlighted in panel B, which all exhibit a lattice spacing of 0.36 nm corresponding to the (101) diffraction planes of anatase TiO$_2$.

nanoparticles exhibited poor crystallinity and high dispersity in size (36—39). Additionally, the formation of snowman-like heterodimers rather than core—shell nanostructures might be ascribed to the asymmetrical surface structures of the gold Janus nanoparticles that provide directional growth of the semiconductor component.

Interestingly, the heterodimer particles exhibit very apparent photoluminescence responses, although TiO$_2$ is a well-known indirect semiconductor and it is generally difficult to observe luminescence emission (from band-edge or trap-state transitions) (40). Figure 2 shows the excitation and emission profiles of the Au—TiO$_2$ heterodimer particles in THF. It can be seen that a broad peak centering around 400 nm appears in the excitation spectrum, which is consistent with the band-gap energy of TiO$_2$ (∼3 eV). It should be noted that the exciton Bohr radius of TiO$_2$ is only 1.5 nm (41), and consequently no apparent quantum confinement effect and blue shift of the band gap is anticipated with the relatively large TiO$_2$ nanoparticles prepared above. When excited at 400 nm, a rather intense emission peak can be observed at 609 nm, which most likely arises from electronic transitions involving trap states. It has to be noted that reports of luminescent TiO$_2$ nanoparticles have been relatively scarce mostly because of low crystallinity and broad size distribution (42—45). In a previous study (46),
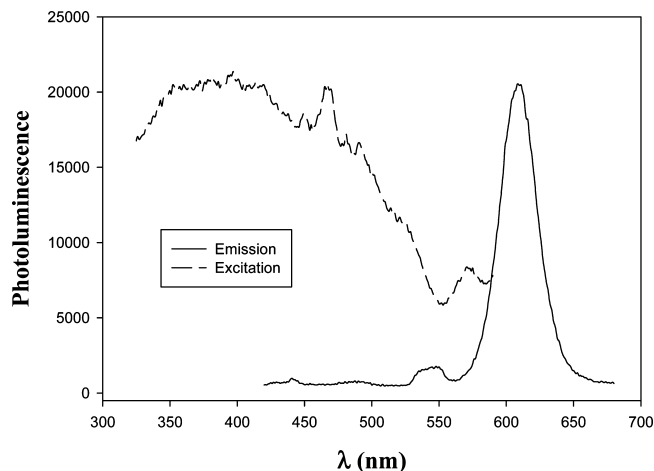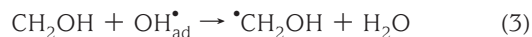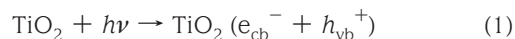
FIGURE 2. Excitation (dashed curve) and emission (solid curve) profiles of the Au−TiO$_2$ heterodimer nanoparticles at a concentration of 0.1 mg/mL in THF.

using a hydrothermal route, Pan and co-workers synthesized TiO$_2$ nanoparticles with core diameters between 4 and 5 nm and observed rather intense photoluminescence near the band edge. Additionally, they observed a relatively weak emission at 732 nm, which was accounted for by the energy loss caused by the self-trapping of excitons through lattice relaxation. A similar observation was reported by Tang et al. (45) with anatase TiO$_2$ thin films and by Ghosh and Adhikari (47) with TiO$_2$ nanoparticles dispersed in micro-emulsion solutions.

The fact that band-edge emission of TiO$_2$ is not ob-served with the above Au−TiO$_2$ heterodimer particles, as compared to the study by Pan and co-workers (46), suggests that there are at least two possible pathways for the photogenerated electrons: (i) rapid decay to the trap states within the TiO$_2$ nanocrystals, which were formed by virtue of bonding interactions with gold nanoparticles (note that the trap-state lifetime is generally much longer than that of the conduction or valence band (47)), and (ii) effective interfacial charge transfer from the TiO$_2$ conduc-tion band to the metal particles (whereas the appearance of an apparent emission at lower energy implies that energy/electron transfer from the TiO$_2$ trap states to gold nanoparticles is not as efficient). If both pathways play a significant role in the overall photoelectron-transfer dy-namics, the Au−TiO$_2$ heterodimers might be exploited as effective photocatalysts, where the efficient separation of photogenerated electrons and holes at the metal−TiO$_2$ interface represents a critical step in the initiation of photocatalytic reduction/oxidation reactions, as mani-fested below.

In this study, the photocatalytic activity of the Au−TiO$_2$ heterodimer nanoparticles prepared above was highlighted by using methanol oxidation into formaldehyde as an il-lustrating example. As mentioned earlier, the heterodimer nanoparticles might be readily dispersed into varied solvent media, rendering them a unique system for homogeneous catalysis that might be monitored photospectrometrically. The reaction mechanism of methanol oxidation has been proposed as follows (24):

$$TiO_2 + h\nu \rightarrow TiO_2 \,(e_{cb}^- + h_{vb}^+) \qquad (1)$$

$$H_2O_{ad} + h_{vb}^+ \rightarrow OH_{ad}^\bullet + H^+ \qquad (2)$$

$$CH_2OH + OH_{ad}^\bullet \rightarrow {}^\bullet CH_2OH + H_2O \qquad (3)$$

$$^\bullet CH_2OH + O_2 \rightarrow HCHO + HO_2^\bullet \qquad (4)$$

Specifically, upon photoirradiation of TiO$_2$ with UV light, electrons are promoted rapidly from the valence band to the conduction band (eq 1). The hole left in the valence band then migrates to the surface of the TiO$_2$ particles and reacts with adsorbed water molecules to form hydroxy radicals (eq 2). These radicals then react with adsorbed methanol to form α-hydroxymethyl radicals (eq 3), which react further with dissolved oxygen to form formaldehyde (eq 4). The forma-tion of formaldehyde is detected by taking advantage of its reaction with acac in the presence of excessive ammonium acetate to form diacetyldihydrolutidine (DDL), a yellow-colored product that exhibits a strong absorbance peak at ~400 nm and thus allows the reaction dynamics to be monitored photospectrometrically (25).

In the above reactions (eqs 1−4), the separation of photogenerated electrons and holes may be facilitated by the close proximity of a gold nanoparticle, which serves as an effective electron sink (the electrons accumulated are most likely involved in the reduction of oxygen into anionic radicals). The key reaction pathways are summarized in Scheme 2.

Figure 3A depicts the UV−vis absorption profiles of the Au−TiO$_2$ heterodimer nanoparticles at a concentration of 0.05 mg/mL in a THF/H$_2$O mixture [1:1 (v/v); total volume 20 mL] with 0.01 M acac, 0.33 M NH$_4$Ac, and 0.62 mM methanol. The spectra were collected after the solution was exposed to UV photoirradiation (365 nm) for different periods of time. Note that, prior to photoirradiation ($t = 0$ min), the absorption profile is essentially featureless, exhib-iting an exponential decay profile that is anticipated for nanometer-sized gold particles. However, after extended photoirradiation, two very well-defined absorption peaks start to grow at 404 and 276 nm. Such a remarkable feature is consistent with the optical characteristics of DDL and thus

Scheme 2. Schematic of Photocatalytic Reactions by Au−TiO$_2$ Heterodimer Nanoparticles
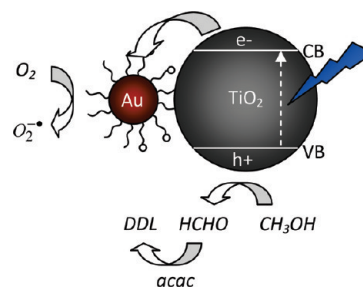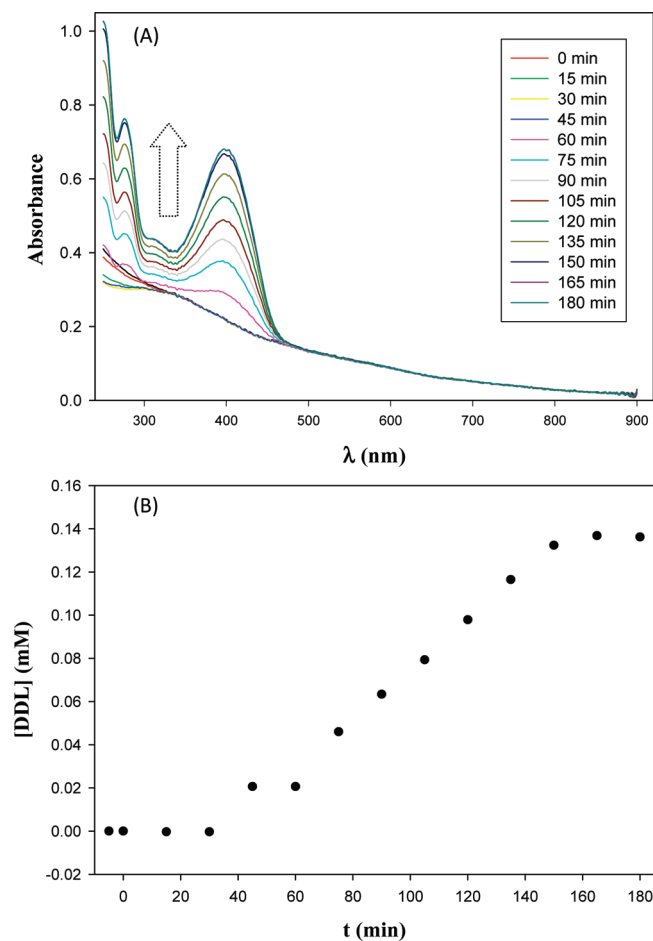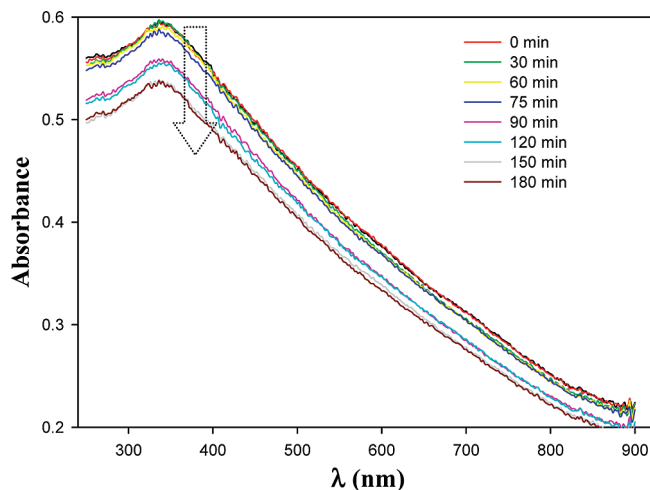
FIGURE 3. (A) UV–vis absorption profiles of the Au–TiO$_2$ heterodimer nanoparticles at a concentration of 0.05 mg/mL in a THF/H$_2$O mixture [1:1 (v/v); total volume 20 mL] with 0.01 M acac, 0.33 M NH$_4$Ac, and 0.62 mM methanol. The spectra were collected after the solution was exposed to UV photoirradiation (365 nm) for different periods of time (shown as figure legends). (B) Variation of the DDL concentration with the photoirradiation time by calibrating the peak absorbance at 404 nm with that of a DDL solution of known concentration.

is strongly indicative of the photocatalytic activity of the Au–TiO$_2$ heterodimer nanoparticles in the oxidation of methanol into formaldehyde (24).

The concentration of DDL formed in the solution was then estimated by calibrating the peak absorbance (at 404 nm) against that of a DDL solution of known concentration. Panel B shows variation of the DDL concentration with the photoirradiation time. It can be seen that, in the first 50 min or so, there was virtually no DDL produced in the solution, suggestive of an induction period for the catalytic activation of the oxidation process. After that, the DDL concentration increases almost linearly with the photoirradiation time, from which the reaction rate constant of DDL formation might be estimated to be 1.12×10^{-3} mM/min, and at approximately 150 min, the DDL concentration reaches a plateau of about 0.14 mM. Because one molecule of DDL is formed by the reaction of two molecules of acac with one molecule of formaldehyde (25), this demonstrates that at least 0.14 mM methanol has been photocatalytically converted into formaldehyde.

FIGURE 4. UV–vis absorption profiles of commercial TiO$_2$ nanoparticles at a concentration of 0.05 mg/mL in a THF/H$_2$O mixture [1:1 (v/v); total volume 20 mL] with 0.01 M acac, 0.33 M NH$_4$Ac, and 0.62 mM methanol. The spectra were collected after the solution was exposed to UV photoirradiation (365 nm) for different periods of time (shown as figure legends).

A control experiment was also carried out with commercial TiO$_2$ nanoparticles (Degussa P25) under otherwise identical experimental conditions to highlight the importance of the incorporation of gold nanoparticles onto the oxide particle surface in promoting charge separation and, consequently, photocatalytic oxidation. Figure 4 shows the UV–vis absorption profile of TiO$_2$ nanoparticles in the presence of acac, NH$_4$Ac, and methanol. Because the particles are not soluble in the reaction media, the optical profiles are mostly due to the scattering of light by TiO$_2$ nanoparticles (the diminishment of the absorbance, as indicated by the dotted arrow, is due to the gradual settling down of the particles from the reaction solution). Nevertheless, it is clear that the characteristic absorption features of DDL are absent even after 180 min of photoirradiation with the same UV light, indicative of the poor activity of TiO$_2$ alone in the photocatalytic oxidation of methanol into formaldehyde.

CONCLUSION

In this study, Au–TiO$_2$ snowman-like heterodimer nanostructures were prepared by a surface sol–gel process based on gold Janus nanoparticles. The resulting heterodimers exhibited well-defined photoluminescence characteristics that were consistent with electronic transitions involving trap states of the TiO$_2$ particles. The photocatalytic activity of the heterodimer particles was highlighted by methanol oxidation into formaldehyde, which was detected photospectrometrically by the Nash method. The enhanced photocatalytic performance, as compared to that of TiO$_2$ nanoparticles alone, was ascribed to the gold nanoparticles, which facilitated charge separation of the photogenerated electrons and holes at the metal–TiO$_2$ interface. These results suggested that (i) there were at least two possible pathways for photogenerated electrons at the TiO$_2$ conduction band, decay to the trap states and transfer to the gold nanoparticles, and (ii) energy/electron transfer from the trap states to gold nanoparticles was less efficient.

Importantly, the ready dispersion of the heterodimer particles into common reaction media provided a chemical environment equivalent to that of homogeneous catalysis for maximal catalytic performance. These unique features suggest that the Au–TiO$_2$ heterodimer nanoparticles might be exploited as effective photocatalysts for the preparation of functional molecules and materials. Furthermore, with the heterdimer structure, both Au and TiO$_2$ are readily accessible and may be further and independently functionalized, leading to the preparation of more complicated functional nanostructures. This will be pursued in future work.

REFERENCES AND NOTES

(1) Solanki, A.; Kim, J. D.; Lee, K. B. *Nanomedicine* **2008**, *3*, 567–578.

(2) Chaim, R.; Levin, M.; Shlayer, A.; Estournes, C. *Adv. Appl. Ceram.* **2008**, *107*, 159–169.

(3) Kitano, M.; Tsujimaru, K.; Anpo, M. *Top. Catal.* **2008**, *49*, 4–17.

(4) Somorjai, G. A.; Park, J. Y. *Chem. Soc. Rev.* **2008**, *37*, 2155–2162.

(5) Greene, L. E.; Yuhas, B. D.; Law, M.; Zitoun, D.; Yang, P. D. *Inorg. Chem.* **2006**, *45*, 7535–7543.

(6) Gratzel, M. *C. R. Chim.* **2006**, *9*, 578–583.

(7) Carp, O.; Huisman, C. L.; Reller, A. *Prog. Solid State Chem.* **2004**, *32*, 33–177.

(8) Demeestere, K.; Dewulf, J.; Van Langenhove, H. *Crit. Rev. Environ. Sci. Technol.* **2007**, *37*, 489–538.

(9) Chen, Q.; Peng, L. M. *Int. J. Nanotechnol.* **2007**, *4*, 44–65.

(10) Fujishima, A.; Honda, K. *Nature* **1972**, *238*, 37–+.

(11) Gratzel, M. *Nature* **2001**, *414*, 338–344.

(12) Gur, I.; Fromer, N. A.; Geier, M. L.; Alivisatos, A. P. *Science* **2005**, *310*, 462–465.

(13) Ohko, Y.; Tatsuma, T.; Fujii, T.; Naoi, K.; Niwa, C.; Kubota, Y.; Fujishima, A. *Nat. Mater.* **2003**, *2*, 29–31.

(14) Xu, J. J.; Zhao, W.; Luo, X. L.; Chen, H. Y. *Chem. Commun.* **2005**, 792–794.

(15) Cozzoli, P. D.; Fanizza, E.; Comparelli, R.; Curri, M. L.; Agostiano, A.; Laub, D. *J. Phys. Chem. B* **2004**, *108*, 9623–9630.

(16) Pastoriza-Santos, I.; Perez-Juste, J.; Carregal-Romero, S.; Herves, P.; Liz-Marzan, L. M. *Chem. Asian J.* **2006**, *1*, 730–736.

(17) Yang, H. Z.; Yang, Y. Q.; Zou, S. Z. *J. Phys. Chem. B* **2006**, *110*, 17296–17301.

(18) Yu, Y. T.; Mulvaney, P. *Korean J. Chem. Eng.* **2003**, *20*, 1176–1182.

(19) Wu, X.-F.; Song, H.-Y.; Yoon, J.-M.; Yu, Y.-T.; Chen, Y.-F. *Langmuir* **2009**, *25*, 6438–6447.

(20) Armelao, L.; Barreca, D.; Bottaro, G.; Gasparotto, A.; Maccato, C.; Maragno, C.; Tondello, E.; Stangar, U. L.; Bergant, M.; Mahne, D. *Nanotechnology* **2007**, *18*, 375709–1.

(21) Chan, S. C.; Barteau, M. A. *Langmuir* **2005**, *21*, 5588–5595.

(22) Buso, D.; Pacifico, J.; Martucci, A.; Mulvaney, P. *Adv. Funct. Mater.* **2007**, *17*, 347–354.

(23) Wang, X. D.; Mitchell, D. R. G.; Prince, K.; Atanacio, A. J.; Caruso, R. A. *Chem. Mater.* **2008**, *20*, 3917–3926.

(24) Ismail, A. A.; Bahnemann, D. W.; Bannat, I.; Wark, M. *J. Phys. Chem. C* **2009**, *113*, 7429–7435.

(25) Nash, T. *Atmos. Environ.* **1967**, *1*, 679–687.

(26) Mori, K.; Hara, T.; Mizugaki, T.; Ebitani, K.; Kaneda, K. *J. Am. Chem. Soc.* **2004**, *126*, 10657–10666.

(27) Marko, I. E.; Giles, P. R.; Tsukazaki, M.; Brown, S. M.; Urch, C. J. *Science* **1996**, *274*, 2044–2046.

(28) Abad, A.; Concepcion, P.; Corma, A.; Garcia, H. *Angew. Chem., Int. Ed.* **2005**, *44*, 4066–4069.

(29) Brauer, G. *Handbook of preparative inorganic chemistry*, 2nd ed.; Academic Press: New York, 1963.

(30) Woehrle, G. H.; Warner, M. G.; Hutchison, J. E. *Langmuir* **2004**, *20*, 5982–5988.

(31) Pradhan, S.; Brown, L. E.; Konopelski, J. P.; Chen, S. W. *J. Nanopart. Res.* **2009**, in press.

(32) Brust, M.; Walker, M.; Bethell, D.; Schiffrin, D. J.; Whyman, R. *J. Chem. Soc., Chem. Commun.* **1994**, 801–802.

(33) Templeton, A. C.; Wuelfing, M. P.; Murray, R. W. *Acc. Chem. Res.* **2000**, *33*, 27–36.

(34) Chen, S. W. *Langmuir* **2001**, *17*, 6664–6668.

(35) Hostetler, M. J.; Wingate, J. E.; Zhong, C. J.; Harris, J. E.; Vachet, R. W.; Clark, M. R.; Londono, J. D.; Green, S. J.; Stokes, J. J.; Wignall, G. D.; Glish, G. L.; Porter, M. D.; Evans, N. D.; Murray, R. W. *Langmuir* **1998**, *14*, 17–30.

(36) Poznyak, S. K.; Talapin, D. V.; Kulak, A. I. *J. Phys. Chem. B* **2001**, *105*, 4816–4823.

(37) Wu, M. M.; Lin, G.; Chen, D. H.; Wang, G. G.; He, D.; Feng, S. H.; Xu, R. R. *Chem. Mater.* **2002**, *14*, 1974–1980.

(38) Kim, C. S.; Moon, B. K.; Park, J. H.; Choi, B. C.; Seo, H. J. *J. Cryst. Growth* **2003**, *257*, 309–315.

(39) Zhou, Y.; Antonietti, M. *J. Am. Chem. Soc.* **2003**, *125*, 14960–14961.

(40) Pankove, J. I. *Optical processes in semiconductors*; Prentice-Hall: Englewood Cliffs, NJ, 1971.

(41) Rodriguez, J. A.; Fernândez Garcia, M. *Synthesis, properties, and applications of oxide nanomaterials*; Wiley-Interscience: Hoboken, NJ, 2007.

(42) Niederberger, M.; Bartl, M. H.; Stucky, G. D. *Chem. Mater.* **2002**, *14*, 4364–4370.

(43) Ramakrishna, G.; Ghosh, H. N. *Langmuir* **2003**, *19*, 505–508.

(44) Zhu, Y. C.; Ding, C. X. *J. Solid State Chem.* **1999**, *145*, 711–715.

(45) Tang, H.; Prasad, K.; Sanjines, R.; Schmid, P. E.; Levy, F. *J. Appl. Phys.* **1994**, *75*, 2042–2047.

(46) Pan, D. C.; Zhao, N. N.; Wang, Q.; Jiang, S. C.; Ji, X. L.; An, L. J. *Adv. Mater.* **2005**, *17*, 1991–1995.

(47) Ghosh, H. N.; Adhikari, S. *Langmuir* **2001**, *17*, 4129–4130.

AM900425V